Strojniški vestnik - Journal of Mechanical Engineering 61(2015)12, 689-697

DOI:10.5545/sv-jme.2015.2794 Original Scientific Paper
Received for review: 2015-06-24
Received revised form: 2015-09-15
Accepted for publication: 2015-10-14

Laser-Induced Deterioration Grinding of Zirconium Oxide (ZrO_2) – Generation of Layer Patterns and Performance Evaluation

Xiaohong Zhang[1,2,*] – Zhaohui Deng[3] – Yinhui Ren[2] – Genyu Chen[2] – Wei Liu[3] – Gaofeng Zhang[4]

[1]Hunan Institute of Science and Technology, College of Mechanical Engineering, China
[2]Hunan University, College of Mechanical and Vehicle Engineering, China
[3]Key Laboratory for High Efficiency and Precision Machining of Difficult-to-Cut Material of Hunan Province, China
[4]Xiangtan University, College of Mechanical Engineering, China

Laser-induced deterioration was proposed for the wet grinding of zirconium oxide (ZrO_2) ceramic used in the dental, semiconductor and automotive industries. The mechanisms for laser induced deterioration and wet grinding of the deterioration layer were theoretically analysed, and the four key processing parameters that determine the micro-topography and distribution of the laser-induced crater were proposed, including the laser power density I_p, the defocus distance z, the laser spot overlap ratio U_s and the laser scanning track line overlap ratio U_l. Further, the forming mechanism of the single pulse-induced crater under different laser power densities, the defocus distance, and the interaction mechanisms between adjacent spots along the longitudinal and transverse directions were investigated. The optimal values of the key processing parameters were identified. To further evaluate the effect of laser-induced deterioration objectively, a comparative experiment was conducted under laser-induced deterioration wet grinding (LIDWG) and conventional grinding (CG) conditions. It was found that the procedure of laser-induced deterioration had a strong influence on the grinding results. The normal and tangential grinding forces for LIDWG condition were lower than for CG condition, with a maximum reduction of 59.2 % (62.9 %).

Keywords: laser-induced crater, deterioration layer, wet grinding, grinding force, zirconium oxide

Highlights

- *The research is focused on analysing the laser-induced deterioration wet grinding of zirconium oxide.*
- *A theoretical study of the micro-topography obtained by laser-induced deterioration under different processing conditions is done.*
- *A uniform distribution of deterioration craters is achieved based on the optimal processing parameters.*
- *An experimental study of the grinding force under different grinding conditions is conducted.*

0 INTRODUCTION

Major advances in the production and application of zirconium oxide (ZrO_2) have been achieved due to their superior properties, such as high thermal strength, hardness, wear resistance, chemical inertness, thermal stability, and high stiffness-to-weight ratio [1]. Diamond grinding and polishing of ZrO_2 have become the most widely used processes in the dental, semiconductor and automotive industries. With the increasing of demand for ZrO_2 products, the widespread use of these materials has been seriously restricted due to the low material removal rate and high processing cost that accounts for more than 75 % of the component cost. The problems associated with precision and efficiency in machining ZrO_2 ceramic have become a significant issue in the manufacturing industry. Rabiey et al. studied novel hybrid bonded diamond tools used to grind zirconium oxide [2]. It was achieved within a selected process window in combination with an elaborate oil cooling system, where material removal was mainly occurring within the ductile cutting mode. A self-sharpening effect of the tool can be observed, and the dressability of the tool further improved the grinding performance. Yan et al. used two-dimensional ultrasonic vibration grinding to machine nano-ZrO_2 and analysed surface quality with or without ultrasonic vibration [3]. The method can improve the surface quality and the life of the diamond wheel. Chen et al. discussed the grinding characteristics and removal mechanisms in the high-speed grinding of ZrO_2 [4]. It was found that the increasing wheel speed can reduce grinding forces due to the reduction of the maximum chip thickness. However, this research mainly focused on the improvement of machining efficiency. The material removal mode was dominated by brittleness removal. In these references, various experiments were carried out on different grinding parameters such as grinding wheel speed, table feed speed, grinding depth, workpiece speed to control surface roughness, residual stresses, and subsurface damage. The rapid blunting and wear of diamond abrasives on the wheel surface may cause frequent redressing and shorten the service life of the grinding wheel [5].

Grinding wheel topography changes during grinding. As a result, the efficiency of the grinding process and the quality of the workpiece are affected

*Corr. Author's Address: College of Mechanical Engineering, Hunan Institute of Science and Technology, China. jansbomb@126.com

negatively most of the time. Wheel wear may induce grinding burn and poor surface quality, even cause serious accidents [6]. Unfortunately, current approaches dealing with wheel wear are based on human experience. The dressing interval is roughly determined, usually by skilled operators. This induces two adverse impacts. Firstly, grinding wheel wear might already happen before the dressing process, which usually causes grinding quality problems. Secondly, if the dressing process is carried out ahead of wheel wear, the grinding efficiency is definitely reduced, and the abrasive materials are simultaneously wasted. Therefore, the material removal behaviour should be mainly plastic deformation and/or ductile removal [7]. Macro-brittle fractures and cracks generated in the grinding mode are not observed. Lower grinding depths and higher wheel speeds were proven to achieve the ductile removal mode. They can also reduce the grinding temperature and the grinding force. However, the disadvantages result in low productivity and high cost.

Laser-assisted machining takes the advantages of local heating and softening of the workpiece by a laser beam in front of the cutting tool. The technique changes the material's behaviour from brittle to ductile. Therefore, it allows difficult-to-machine materials to be machined with greater cutting depth [8] and [9]. In traditional laser-assisted grinding (LAG), the material is heated by a laser prior to the material removal location. Thus, the method permits high stock removal rates [10] and [11]. If the thickness of the heating layer is greater than the grinding depth, the crack may remain in the subsurface, which greatly affects the properties of the machined part. In particular, one of the key factors is the tool-beam distance where the laser beam is positioned to achieve a uniform temperature distribution at the cutting edge without burning the grinding wheel. For a shorter distance, the temperature might not be high enough, and the grinding wheel will be burnt. In contrast, for a longer distance, this process might cause serious surface/subsurface damage in the workpiece. An additional process such as polishing should be added to eliminate this damage. Additionally, the characteristics of traditional LAG limit the use of coolant and also cannot fundamentally eliminate surface/subsurface cracks due to heat accumulation [12] and [13]. These problems have become the bottleneck limiting the application of LAG [14] and [15].

In this paper, a strategy for laser-induced deterioration in the wet grinding of ZrO_2 ceramic has been proposed. Some key processing parameters that determine the micro-topography and distribution of the deterioration layer were discussed based on the forming mechanisms of the single pulse-induced crater and the interaction mechanisms between adjacent spot. A pulsed fibre laser was used to achieve the uniform distribution of deterioration craters by reasonably controlling the average laser power P_{avg}, the defocus distance z, the laser spot overlap ratio U_s and the laser scanning track line overlap ratio U_l. Then, a three-dimensional (3D) microscope with an ultra-large depth-of-field (ULDF) was used to observe the generation of single pulse-induced craters, and the arrangement and distribution of combinations of craters. In particular, the differences in grinding forces obtained under laser-induced deterioration wet grinding (LIDWG) and conventional grinding (CG) conditions were compared and discussed.

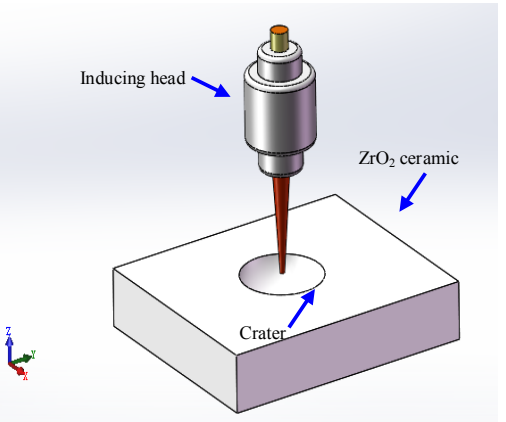

Fig. 1. *Schematic of laser induced deterioration*

The objective of LIDWG is to produce uniform deterioration layer patterns appropriate to a high efficiency grinding task. LIDWG involves two different sub-processes: deterioration and grinding. For conventional LAG, softening and grinding should be done simultaneously. However, for LIDWG, especially in order to integrate the advantages of grinding fluid, deterioration and grinding are performed in two distinct steps [16] and [17]. The first step of LIDWG is briefly illustrated in Fig. 1. As shown in Fig. 1, during the deterioration stage a pulsed incident laser beam was sent in the vertical direction of the workpiece surface. A significant fraction of the incident light energy was absorbed by the workpiece. High-temperature gradients can be caused by intense laser radiation [18]. A multi-axis numerical control (NC) system was applied to precisely control the laser beam while it scanned along the surface of the workpiece. It will lead to the emergence of the deterioration layer. Then, the deterioration layer

was formed within the surface/subsurface of the workpiece. The distribution of the deterioration layer can be made uniform by selecting optimum processing parameters. The laser power density becomes low, indicating that the laser energy is passing through the workpiece surface without forming the desired depth of the deterioration layer. The repeated scanning is necessary until the desired deterioration depth is reached. The mechanism of laser-induced deterioration is to heat, melt, and deteriorate the ceramic material; some of which will also be directly vaporized and decomposed. In contrast, if the laser power density is too high, excess heat will be transferred to the interior of the workpiece. The thermal stress gradient from the workpiece surface to the bottom of the chip is increased. It leads to thermal microcracks, which can severely affect the mechanical properties and surface integrity of the workpiece. In a word, the depth of the deterioration layer should not exceed the grinding allowance.

1 EXPERIMENTAL APPROACH AND PROCEDURE

1.1 Laser-Induced Deterioration Grinding

A cross-section micrograph of induced craters is shown in Fig. 2. H is the depth of the deterioration layer. For the same laser model, the micro-topography of single pulse-induced craters depends on the laser power density I_p and the defocus distance z. The three equations are utilized to calculate the values of the processing parameters including I_p, U_s and U_l.

$$I_P = \frac{4P_m}{\pi d_0^2 f \tau}, \quad (1)$$

$$U_S = \frac{d_0 - S}{d_0} \times 100\%, \quad (2)$$

$$U_L = \frac{d_0 - L}{d_0} \times 100\%. \quad (3)$$

For example, the value of I_p is determined by the four parameters, including average laser power P_{avg}, the pulse frequency f, the diameter of the laser spot on the workpiece surface d_0 and the pulse width τ. Similarly, the ZrO_2 ceramic surface topography generated by pulsed laser depends on the appropriateness of the micro-topography of single pulse-induced craters, the arrangement and distribution of a large number of craters, and the depth of the deterioration layer. The arrangement and distribution of a large number of craters are determined by two processing parameters: U_s and U_l. U_s is the overlap ratio of two adjacent laser spots in the same laser scanning track line. U_l is the overlap ratio of two adjacent scanning tracks on the surface of the workpiece. Considering that the thermal influence mechanism between two adjacent laser spots of different directions is similar, so U_s and U_l are set to equal. This means that three main processing parameters I_p, z, and U_s are very important for the quality of the laser-induced deterioration.

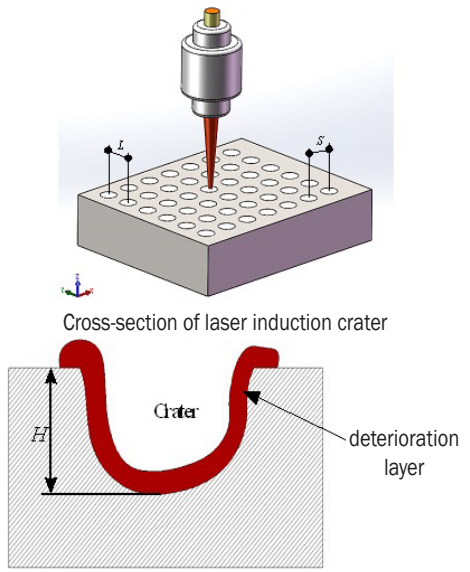

Fig. 2. *Schematic of the micro-topography and distribution of induced craters*

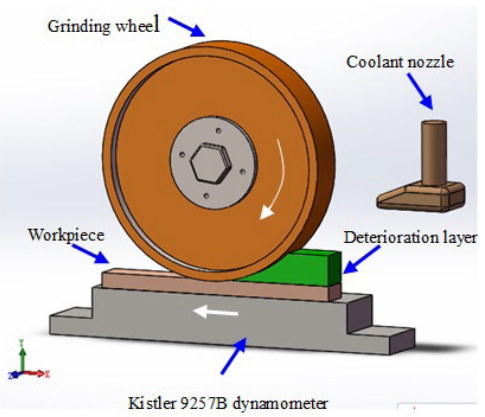

Fig. 3. *Schematic of wet grinding of the deterioration layer*

As shown in Fig. 3, the deterioration layer with a number of laser craters on the workpiece can be removed in the down-grinding mode. In contrast to the traditional grinding process of ZrO_2 ceramic, higher material grinding rates can be achieved. It is possible to avoid a bigger grinding force, a higher grinding temperature, grinding wheel wear, grinding

wheel wear-related or brittle removal mode-related errors. The kinematic parameters of wheel speed (V_s), grinding depth (a_p), and workpiece velocity (V_w) were designed to ensure the whole wet grinding stage could be of high efficiency and high quality.

1.2 Experimental Procedures

The experiment was conducted in two stages. The first stage was the laser-induced deterioration experiment for the ZrO_2 engineering ceramic specimens. The experimental parameters are listed in Table 1a). The deterioration layer surface micro-topography was measured using a 3D ULDF microscope (Model: VHX-S1000) to determine the optimal deteriorating parameters. The second stage was the wet grinding experiment, performed using the processing parameters in Table 1b. Grinding forces in both normal and tangential directions were measured using a dynamometer (Kistler Instrument Corporation, type Kistler 9257B) fixed on the machine table. Surface roughness was measured by a surface coarseness profiling instrument (Type Homel18000) made in Germany.

Table 1. *The experimental parameters of LIDWG*

a) Laser-induced deterioration	
Pulse frequency, f	70 kHz
Average laser power, P_{avg}	25 W to 50 W
Defocus distance, z	0 mm to 2 mm
Track line overlap ratio, U_s	–300 % to 80 %
b) Wet grinding	
Wheel speed, V_s	80 m/s
Grinding depth, a_p	10 μm to 50 μm
Workpiece velocity, V_w	50 mm/s

1.3 Experimental Apparatus and Materials

Fig. 4 shows the apparatus used for the pulsed laser-induced deterioration grinding. A compact pulsed ytterbium-doped fibre laser (Model: YLP-1/120/100/100-HC) was adopted in the experiment. This laser has an average power (P_{avg}) of 10 W to 100 W, a pulse frequency (f) of 50 kHz to 150 kHz, a pulse width (τ) of 210 ns, and a wavelength (λ) of 1,064 nm. The laser energy output has an approximately Gaussian distribution. The laser beam was transmitted to the inducing head with a standard isolator fixed on a 2D motorized translation stage (Model: 7STA01A), using a single-mode fibre, and is then focused using a lenticular lens with a focal length of 180 mm inside the inducing head. The beam struck the working surface of the ZrO_2 ceramic with a defocusing amount of 2 mm and a spot diameter (d_0) of approximately 180 μm. During the laser induced deterioration experiment, a gas nozzle with an inner diameter of 4 mm provided auxiliary lateral blowing air at a pressure of 0.1 MPa. The purpose is to remove any molten material and observe the micro-topography of induced craters easily.

Fig. 4. *a) The apparatus used for laser induced deterioration grinding; b) a detail*

Surface grinding experiments were employed in the down-grinding mode on a high-speed grinder (HGS-II 8000). The spindle is capable of running up to 8000 rpm. The grinding wheel was a diamond grinding wheel of type SDC80N100B. Grinding force signals were recorded by a personal computer via a data acquisition system and then filtered with LABVIEW software. The grinding wheel was dressed by an electroplated diamond roller dresser (Type S-DC-C-110×12×28) in down dressing mode. During grinding, a 3% solution of water-based coolant (Type W20) was applied. The ground surfaces were cleaned with alcohol.

The experimental specimens used in this paper are the ZrO_2 ceramic produced by Yixing Shanjia Company (China). The purity of the ZrO_2 ceramic is 95 %, with a density of 5900 kg/m³, Young's modulus of 200 GPa, a thermal conductivity of 3 W/(m·K), and hardness of 1400 HV. The dimensions of the workpiece are 20 mm × 30 mm × 10 mm.

2 RESULTS AND DISCUSSION

2.1 Laser Induced Deterioration Experiment

2.1.1 Impact of the Laser Power Density on the Micro-Topography

For laser-induced deterioration, the main purpose is to obtain the ideal deterioration layer on the top of the whole surface of ZrO_2 ceramic. Moreover, the distribution of the craters is uniform, and the thickness of deterioration layer is constant. The laser power density I_p and the defocus distance z belong to the most important processing parameters. They are closely related to the geometrical dimension and topography of the induced craters. That is to say, the quality and accuracy of laser induced deterioration are determined by the values of the laser power density and the defocus distance. Of course, it also determines the success or failure of the later period of wet grinding. As shown in Fig. 2, the four parameters were given as fixed values besides the laser power density I_p and the defocus distance z in order to analyse the influence mechanism more accurately. Therefore, to better understand the characteristics of laser-induced deterioration, a variety of trials were carried out by varying the laser power from 25 W to 50 W and the defocus distance from 0 mm to 2 mm for the pulse frequency of 70 kHz, the spot diameter of 0.18 mm and the pulse width of 210 ns.

Fig. 5 shows the micro-topography of a single pulsed laser-induced crater with different average laser powers and defocus distances. Due to the Gaussian nature of the laser beam, the temperatures at the center of the radiation zone exceed the melting temperature of the ZrO_2 ceramic. It can be found from Fig. 5a that when the average power was 25 W and the defocus distance was 2 mm, because of the low corresponding laser power density of 5.29×10^7 W/cm², a small portion of the ZrO_2 ceramic material in the radiation zone deteriorated and was removed mainly through melting, combined with vaporization. This resulted in a small single pulse-induced crater and low laser-induced deterioration efficiency. The

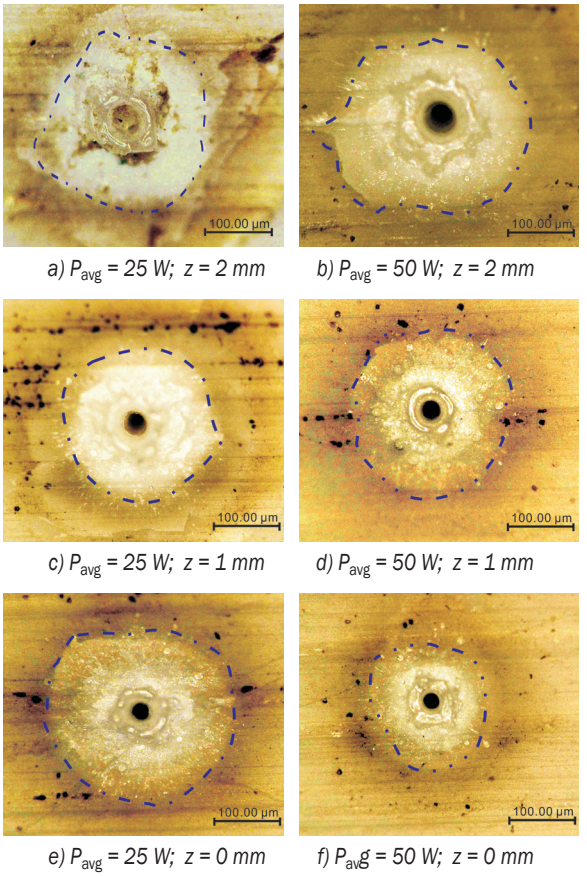

a) P_{avg} *= 25 W; z = 2 mm* *b)* P_{avg} *= 50 W; z = 2 mm*

c) P_{avg} *= 25 W; z = 1 mm* *d)* P_{avg} *= 50 W; z = 1 mm*

e) P_{avg} *= 25 W; z = 0 mm* *f)* P_{avg} *= 50 W; z = 0 mm*

Fig. 5. *The micro-topography of a single pulsed laser-induced crater*

volume and depth of the induced crater was especially trivial. The cause of this failure was the average power being lower and the defocus distance being larger. The temperatures at the center of the radiation zone reached the threshold of heating, melting, and deteriorating the ZrO_2 ceramic material. However, it was insufficient to form an adequate deterioration layer, leaving a shallow and small pit on the surface. As displayed in Fig. 5b, when P_{avg} reached 50 W, corresponding to the laser power density of 10.58×10^7 W/cm², a significant crater can be observed on the ZrO_2 ceramic surface. A larger volume of molten ZrO_2 ceramic spilled outward at greater speeds from the bottom of the crater. The melted material can form a recast layer. Its extension is clearly marked with a blue dotted line. As the defocus distance was gradually decreases within the range from 2 mm to 0 mm, as shown in Fig. 5c to f, the depth of craters increases and the width of craters decreases. When the defocus distance is set to 0, a crater of high depth-diameter ratio will be formed because of energy concentrated in a small

range of spot. The molten material is difficult to climb along the sidewalls of the hole and splash out of the pit. Thus, it is necessary to select a larger value for ensuring a removal area under a certain laser power. Therefore, the volume and depth of the single pulse-induced crater and the laser-induced deterioration efficiency gradually increased with the increasing of the laser power on the premise of a constant defocus distance. They gradually increased with the increasing of the defocus distance on the premise of a constant laser power. Fig. 5d shows that when the average laser power was further increased to 50 W and the defocus distance was set to 1 mm, the volume and depth of the single pulse-induced crater were relatively ideal.

Therefore, a defocus distance of 1mm and an average laser power of 50 W (P_{avg}) was optimal for the pulsed laser induced deterioration of the ZrO_2 ceramic. However, the interaction mechanism of two adjacent laser spots should be investigated, because an excessively high overlap ratio can cause an excessively thermal accumulation in the spot overlap zone. If the depth of the deterioration layer is less than the grinding allowance, it is allowed and beneficial for high efficient processing. Nevertheless, if it is greater than, it will be harmful and could directly cause serious surface damage, or even destroy it.

2.1.2 Impacts of the Overlap Ratios U_s on the Micro-Topography

The forming mechanism of the single pulse-induced crater under different laser power density can only be understood with the analysis of the impact of the laser power densities on the micro-topography. However, during the laser induced deterioration of the ZrO_2 ceramic, the laser outputs a series of laser pulse sequences. In order to achieve the uniform distribution of deterioration craters, improve the grinding efficiency, and reduce the material collapse and grinding wheel wear, it is necessary to reveal the interaction mechanism of two adjacent laser spots. Choosing a suitable laser spot overlap ratio of two adjacent laser spots U_s is the basis for generating the laser pulse-induced craters to cover the entire surface of the ZrO_2 ceramic. An excessively high overlap ratio should not be allowed. It can aggravate surface/subsurface cracks due to the heat accumulation effect. This results in the lower efficiency of laser induced deterioration or even the burning or scrapping of the workpiece.

Fig. 6 displays the micro-topography of laser-induced craters under different laser spot overlap ratio U_s. In the figure, a variety of trials was carried out

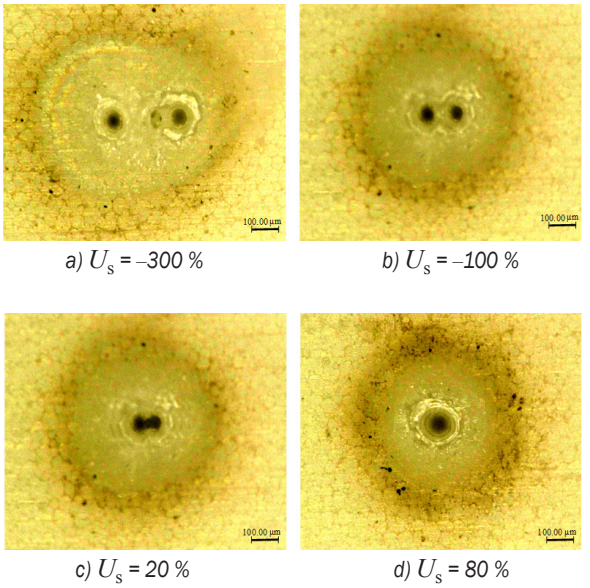

a) U_s = –300 % b) U_s = –100 %

c) U_s = 20 % d) U_s = 80 %

Fig. 6. *The micro-topography of laser-induced craters under different laser spot overlap ratio U_s*

by varying the overlap ratio from -300 % to 80 % for the laser power of 50 W and the defocus distance of 1 mm. Obviously, the lowest low-lying area is the center of the laser-induced crater, and the highest area is the recast layer locating around the crater. It can be found from Fig. 6a that when the laser spot overlap ratio was –300 %, there was no obvious influence between the two adjacent craters due to the far center distance. Fig. 6b shows that when the laser spot overlap ratio was –100 %, the single pulse-induced craters on the ZrO_2 ceramic were approximately dispersed distribution. The material between the two adjacent craters was not vaporized or deteriorated. It cannot reduce the difficulty of the subsequent grinding process. As shown in Fig. 6c, the single pulse-induced craters were connected. The straightness of the induced crater's boundary gradually improved, because a higher laser spot overlap ratio U_s caused increased arrangement density of the single pulse-induced craters and increased uniformity of the laser-induced deterioration efficiency of the ZrO_2 ceramic material in the radiation zone, thus improving the surface quality after deterioration. In particular, the recast layer around the second laser-induced crater was irregular. This phenomenon is attributed to the thermal effect caused by the first laser-induced process. Fig. 6d shows that when the laser spot overlap ratio was 80 %, only one crater can be observed, and its shape is elliptical. The main reason is due to the higher overlap ratio. This will result in a great reduction of

deterioration processing efficiency. Therefore, under the current experimental conditions, an overlap ratio of 20 % was optimal for the pulsed laser induced deterioration of the ZrO_2 ceramic.

2.1.3 Deterioration Experiment

It can be known from the above analysis that a suitable laser spot overlap ratio of two adjacent laser spots U_s only guarantees achieving the uniform distribution of deterioration craters in the same laser scanning track line. For the entire surface of the ZrO_2 ceramic, using a suitable overlap ratio of two adjacent scanning tracks U_l is the key procedure for generating a uniform distribution deterioration layer. Considering that the interaction mechanisms between adjacent spots along the longitudinal and transverse directions are approximately the same, the overlap ratios U_s and U_l are set to be equal. Fig. 7 displays the micro-topography of laser induced craters under laser spot overlap ratios U_s and U_l of 20 %. In order to observe clearly the result of the experiment, the number of the spot along the longitudinal direction was set to 2. It is indicated that a large area of the material was deteriorated, resulting in significant uniformity of deterioration layer distributions. The optimal result of the distribution of the deterioration layer can be achieved.

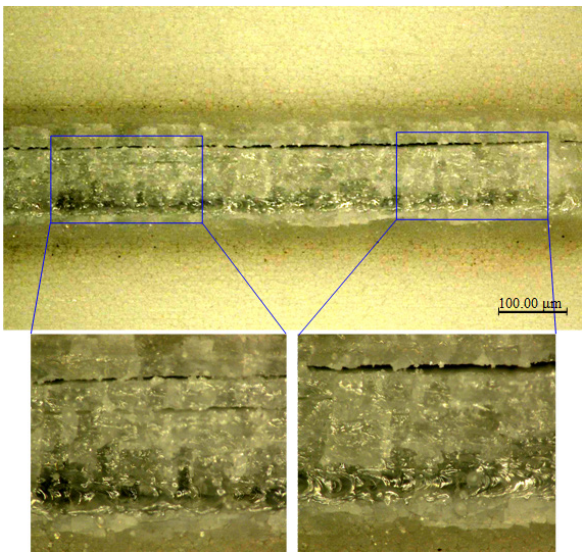

Fig. 7. *The micro-topography of laser-induced craters under laser spot overlap ratio Us and Ul of 20 %*

2.2 Wet Grinding of the Deterioration Layer Experiment

Finally, to further objectively evaluate the performance of laser-induced deterioration, a comparative experiment was conducted under CG and LIDWG conditions. The relationships between the normal and tangential grinding forces (F_t and F_n) to the grinding depth (a_p) during grinding were measured using a dynamometer (Kistler Instrument Corporation, type Kistler 9257B) fixed on the machine table, as shown in Fig. 8a and b, respectively. To better understand the characteristics of LIDWG, a variety of trials were carried out by varying the grinding depth from 10 µm to 50 µm for a workpiece velocity of 50 mm/s and a grinding wheel speed of 80 m/s.

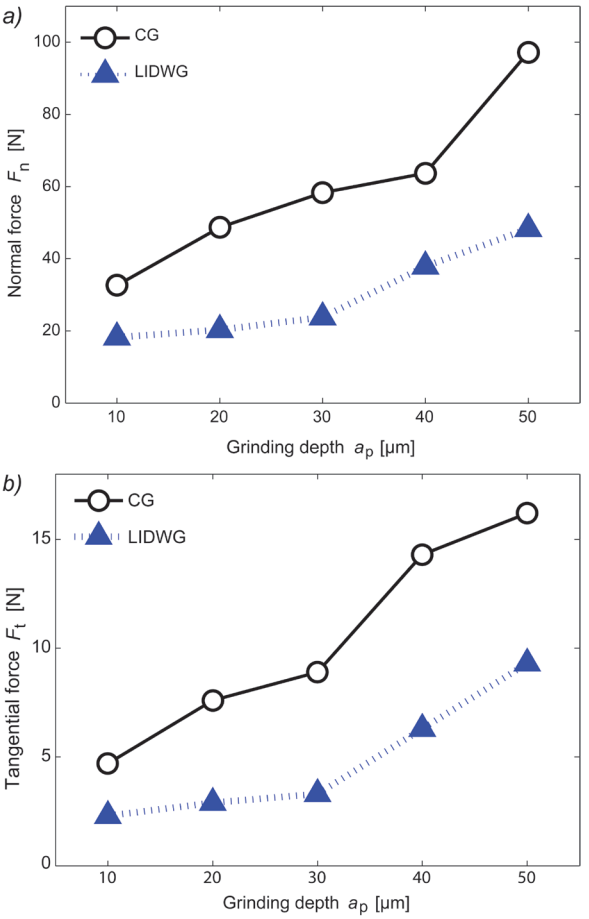

Fig. 8. *The relationship between the grinding force and the grinding depth under CG and LIDWG conditions, a) normal force, b) tangential force*

Fig. 8 shows that the normal and tangential grinding forces at the LIDWG condition were lower than at the CG condition. Furthermore, the normal and tangential grinding forces increased in response to increasing the grinding depth, as expected. This relationship should be attributed to the increasing in the non-deformed chip thickness at greater grinding depths. For the same grinding depth of 10 µm, the average normal (tangential) grinding forces for the

LIDWG condition were 44.2 % (51.1 %) lower than for the CG condition. Similarly, the average normal grinding forces for the LIDWG condition were 58.3 % (61.8 %) lower for a grinding depth of 20 μm and 59.2 % (62.9 %) lower for a grinding depth of 30 μm. The average normal grinding forces for the LIDWG condition were 40.5 % (55.9 %) lower for a grinding depth of 40 μm and 50.3 % (42.6 %) lower for a grinding depth of 50 μm.

A possible reason for this finding is the fact that the deterioration layer has some characteristics, such as loose structure and low strength, and it is also easy to be remove by grinding. In particular, the workpiece surface after laser-induced deterioration was not flat. Compared with CG condition, the amount of grinding removal material was smaller and similar to the intermittent grinding to some extent under LIDWG condition. When grinding a workpiece, the induced craters can result in a decreased contact area between the wheel and the workpiece. Simultaneously, it was found that the craters had the ability to store grinding fluid. This process caused less friction and contact, which eventually decreases the grinding force. In contrast, in the LIDWG condition the removal mode could be transited from a larger scale fracture mode to a smaller scale one. Especially when the grinding depth was less than the thickness of the deterioration layer, the brittle fracture mode could also be changed to a ductile flow. The diamond grinding wheel was not easily blunted. Consequently, less friction and better lubrication/cooling effect were produced between the surfaces of the grinding wheel and the workpiece, i.e., with smaller normal and tangential grinding forces.

3 CONCLUSIONS

In this study, a strategy for laser-induced deterioration in the wet grinding of ZrO_2 ceramic has been proposed. The mechanisms of laser induced deterioration and wet grinding of the deterioration layer were theoretically analysed. A series of laser-induced deterioration experiments and wet grinding experiments were performed on LIDWG and CG conditions, respectively. The uniform distribution of deterioration craters can be achieved by reasonably controlling the laser power density I_p, the defocus distance z, the laser spot overlap ratio U_s and the laser scanning track line overlap ratio U_l. The four key processing parameters ultimately determine the quality and accuracy of the deterioration layer, as well as the success or failure of the later period of wet grinding. The micro-topography of a single pulsed laser-induced crater with different average laser powers and different overlap ratios was measured using a 3D ULDF microscope. When the average laser power (P_{avg}) was 50 W and the corresponding laser power density (I_p) was approximately 10.58×10^7 W/cm², the pulsed laser induced deterioration of the ZrO_2 ceramic yielded satisfactory deterioration quality and less surface damage. The uniform distributions of laser-induced craters under different overlap ratios U_s and U_l is be achieved when their values were 20 %. The comparative grinding experiment indicates that the strategy has been proved effective. The normal and tangential grinding forces for the LIDWG condition were lower than for the CG condition, with a maximum reduction of 59.2 % (62.9 %) for the maximum average normal (tangential) grinding forces, separately. It was attributed to less friction and better lubrication/cooling effect on the basis of the removal mode transition and the ability of craters to store grinding fluid.

4 ACKNOWLEDGEMENT

The authors are grateful for the financial support from the National Natural Science Foundation of China (Grant No. 51405158) and the Open Foundation for High Efficiency and Precision Machining of Difficult-to-Cut Material of Hunan Province (Grant No. E21432). The first author would like to thank Mr. X.Y. Zhao for their experimental support and analysis assistance.

5 REFERENCES

[1] Xie, G.Z., Huang, H. (2008). An experimental investigation of temperature in high speed deep grinding of partially stabilized zirconia. *International Journal of Machine Tools and Manufacture*, vol. 48, no. 14, p. 1562-1568, **DOI:10.1016/j.ijmachtools.2008.06.002**.

[2] Rabiey, M., Jochum, N., Kuster, F. (2013). High performance grinding of zirconium oxide (ZrO2) using hybrid bond diamond tools. *CIRP Annals-Manufacturing Technology*, vol. 62, no. 1, p. 343-346, **DOI:10.1016/j.cirp.2013.03.073**.

[3] Yan, Y.Y., Zhao, B., Liu, J.L. (2009). Ultraprecision surface finishing of nano-ZrO2 ceramics using two-dimensional ultrasonic assisted grinding. *International Journal of Advanced Manufacturing Technology*, vol. 43, no. 5-6, p. 462-467, **DOI:10.1007/s00170-008-1732-x**.

[4] Chen, J., Shen, J., Huang, H., Xu, X.P. (2010). Grinding characteristics in high speed grinding of engineering ceramics with brazed diamond wheels. *Journal of Materials Processing Technology,* vol. 210, no. 6-7, p. 899-906, **DOI:10.1016/j.jmatprotec.2010.02.002**.

[5] Zhang, X.H., Yan, C., Chen, G.Y., An, W.K., Deng, Z.H. (2014). Experimental investigations of microcracks in laser induced cracking turning alumina ceramic. *Materials and*

Manufacturing Processes, vol. 29, no. 10, p. 1277-1283, **DOI:10.1080/10426914.2014.930884**.

[6] Uhlmann, E., Hoghé, T., Kleinschnitker, M. (2013). Grinding wheel wear prediction at double face grinding with planetary kinematics using analytic simulation. *International Journal of Advanced Manufacturing Technology*, vol. 69, no. 9-12, p. 2315-2321, **DOI:10.1007/s00170-013-5197-1**.

[7] Tsai, M.Y., Jian, S.X. (2012). Development of a micro-graphite impregnated grinding wheel. *International Journal of Machine Tools and Manufacture*, vol. 56, p. 94-101, **DOI:10.1016/j.ijmachtools.2012.01.007**.

[8] Ding, H., Shin, Y.C. (2013). Improvement of machinability of Waspaloy via laser-assisted machining. *International Journal of Advanced Manufacturing Technology*, vol. 64, no. 1-4, p. 475-486, **DOI:10.1007/s00170-012-4012-8**.

[9] Singh, G., Teli, M., Samanta, A., Singh, R. (2013). Finite Element Modeling of Laser-Assisted Machining of AISI D2 Tool Steel. *Materials and Manufacturing Processes*, vol. 28, no. 4, p. 443-448, **DOI:10.1080/10426914.2012.700160**.

[10] Westkamper, E. (1995). Grinding assisted by Nd:YAG lasers. *CIRP Annals-Manufacturing Technology*, vol. 44, no. 1, p. 317-320, **DOI:10.1016/S0007-8506(07)62333-6**.

[11] Kumar, M., Melkote, S., Lahoti, G. (2011). Laser-assisted microgrinding of ceramics. *CIRP Annals-Manufacturing Technology*, vol. 60, no. 1, p. 361-370, **DOI:10.1016/j.cirp.2011.03.121**.

[12] Mao, C., Tang, X.J., Zou, H.F., Huang, X.M., Zhou, Z.X. (2012). Investigation of grinding characteristic using nanofluid minimum quantity lubrication. *International Journal of Precision Engineering and Manufacturing*, vol. 13, no. 10, p. 1745-1752, **DOI:10.1007/s12541-012-0229-6**.

[13] Guo, B., Zhao, Q., Fang, X. (2014). Precision grinding of optical glass with laser micro-structured coarse-grained diamond wheels. *Journal of Materials Processing Technology*, vol. 214, no. 5, p. 1045-1051, **DOI:10.1016/j.jmatprotec.2013.12.013**.

[14] Kim, H.C., Ko, T.J. (2015). Verification of simulation of surface texturing on planar surface by grinding. *International Journal of Precision Engineering and Manufacturing*, vol. 16, no. 2, p. 225-231, **DOI:10.1007/s12541-015-0030-4**.

[15] Rabiey, M., Walter, C., Kuster, F., Stirnimann, J., Pude, F., Wegener, K. (2012). Dressing of hybrid bond CBN wheels using short-pulse fiber laser. *Strojniški vestnik - Journal of Mechanical Engineering*, vol. 58, no. 7-8, p. 462-469, **DOI:10.5545/sv-jme.2011.166**.

[16] Walter, C., Komischke, T., Kuster, F., Wegener, K. (2014). Laser-structured grinding tools – generation of prototype patterns and performance evaluation. *Journal of Materials Processing Technology*, vol. 214, no. 4, p. 951-961, **DOI:10.1016/j.jmatprotec.2013.11.015**.

[17] Grigoriev, S.N., Starkov, V.K., Gorin, N.A., Krajnik, P., Kopac, J. (2014). Creep-feed grinding: an overview of kinematics, parameters and effects on process efficiency. *Strojniški vestnik - Journal of Mechanical Engineering*, vol. 60, no. 4, p. 213-220, **DOI:10.5545/sv-jme.2013.1547**.

[18] Sušnik, J., Šturm, R., Grum, J. (2012). Influence of laser surface remelting on Al-Si alloy properties. *Strojniški vestnik - Journal of Mechanical Engineering*, vol. 58, no. 10, p. 614-620, **DOI:10.5545/sv-jme.2012.696**.